Bounded Orbits near Binary Systems Comprised of Small Irregular Bodies

Loic Chappaz* and Kathleen Howell†
Purdue University, West Lafayette, Indiana, 47906, USA

To investigate the behavior of a spacecraft near a pair of irregular bodies, consider a three body configuration (one massless). Two massive bodies, P_1 and P_2, form the primary system; each primary is modeled as a sphere or an ellipsoid. Concepts and tools similar to those applied in the Circular Restricted Three-Body Problem (CR3BP) are exploited to construct periodic trajectories for a third body in synchronous systems; such orbits are also leveraged to design even more complex trajectories. An alternative approach where the primaries are modeled as geometric polyhedra is also discussed.

I. Introduction

While most of the more massive bodies in the solar system are reasonably spherical, there are many smaller objects with very irregular shapes. Such small bodies may orbit the Sun, a planet, or even an asteroid or other small body. These irregular objects are the focus of increasing scientific interest and their study, through various types of observations, offers insight into the early development of the solar system, as well as the formation and origin of more massive bodies. However, ground-based observations possess limited capabilities and closer observations, available during in situ missions, supply higher volume and higher quality data for analysis. Yet, to successfully design trajectories to reach such small, arbitrarily-shaped bodies and to explore the nearby regions, a more thorough understanding of the dynamical environment in the vicinity of such systems is required.

In recent years, several spacecraft have been delivered to the vicinity of small irregular bodies and more complex missions are under development. In 2001, after a series of orbital revolutions to bring the NEAR spacecraft closer to the asteroid 433 Eros and to gather more scientific observations, the vehicle landed on the asteroid surface.[1] Launched in 2007, the current Dawn project is another mission to multiple irregular bodies, with a spacecraft that orbited Vesta for over a year and is now enroute to the dwarf planet Ceres.[2] The Russian Phobos-Grunt spacecraft, launched in November 2011, originally planned to land a probe on Phobos and return a soil sample to Earth; unfortunately, the spacecraft never left Earth orbit.[3] In 2016, the NASA mission OSIRIS-REX is scheduled to deliver a spacecraft to the asteroid 1999 RQ36 to collect soil samples and to investigate this potentially hazardous object.[4] Based on such initial steps, the number of proposals involving such spacecraft destinations is generally increasing. In addition, current estimates indicate that approximately sixteen percent of the known near-Earth asteroid population may be binaries[5] and a few new mission concepts are emerging to visit binary systems comprised of irregular bodies. Thus, further exploration of the dynamical behavior in such an environment is warranted. In support of such future endeavors, previous analyses have investigated the dynamical environment in the vicinity of a pair of irregularly-shaped bodies with a similar ellipsoid-sphere model,[6,7] and some investigations have been completed with alternative approaches that are based on modeling of the primary bodies as a geometric polyhedron.[8,9] Such models have also been previously applied to scenarios that involve a single asteroid.[10]

The focus of this analysis is the behavior of a third body in the vicinity of a system comprised of two irregular bodies. There are three major objectives: (i) survey of the design space through the computation of a large set of families of periodic orbits employing increasingly complex dynamical models and identification

*Ph.D Student, School of Aeronautics and Astronautics, Purdue University, 701 W Stadium Ave., West Lafayette, IN 47906; Member AAS, AIAA.

†Hsu Lo Distinguished Professor, School of Aeronautics and Astronautics, Purdue University, 701 W Stadium Ave., West Lafayette, IN 47906; Fellow AAS, AIAA.

of trajectories with particular interest for mission scenarios that involve the exploration of the primary bodies or the nearby regions, (ii) exploitation of such orbits, develop an automated tool to construct third-body trajectories that exhibit some desired characteristics to produce baseline trajectories for such mission scenarios, (iii) complete an initial assessment of the robustness of such solutions under more realistic simulation conditions. Initially, the familiar Circular Restricted Three Body Problem (CR3BP) is employed, that is, a model where the primary bodies are modeled as point masses. Within the context of exploring third-body trajectories in the vicinity of two small irregular bodies, two spherical primaries may not, in general, be a reasonable assumption. This more specific problem motivates the introduction of a dynamical model that incorporates more complexity in the primary system model. As a first step, one primary is modeled as a massive ellipsoid rather than a point mass, that is, a sphere-ellipsoid system. Then, the complexity of the model is increased again and both primaries are ellipsoidal, or, an ellipsoid-ellipsoid system. To explore the dynamical behavior of a third body near such systems, periodic orbits are of special interest. In the CR3BP, a wide variety of periodic trajectories that exhibit distinct characteristics are well known. For sphere-ellipsoid and ellipsoid-ellipsoid systems, a synchronous primary configuration represents a system that is analogous to the CRTBP, with one or two ellipsoidal primaries rather than point masses. Thus, concepts and tools similar to those applied in the CRTBP are available. Finally, in an initial effort to assess the feasibility and robustness of the trajectories produced with the idealized dynamical models, these solutions are converged into a higher fidelity model where each primary is modeled as a geometric polyhedron.

II. Dynamical Models Development

Within the context of trajectory exploration of systems comprised of small irregular bodies, a first step in the analysis is the development of a dynamical model that describes the motion of the primary system. Then, to incorporate the motion of a third body, additional dynamical models that describe the third-body behavior for different levels of complexity in the primary system model are constructed.

II.A. Circular Restricted Three-Body Problem (CRTBP)

II.A.1. Motion of the primary system

In the CRTBP, the two primaries are point masses, labeled P_1 and P_2 with masses m_1 and m_2, respectively. The mass parameter of the system is defined as $\mu = \frac{m_2}{m_1+m_2}$ and the orbits of the two bodies are assumed to be coplanar and circular relative to the system barycenter. A barycentric rotating frame is defined such that the z-axis is aligned with the angular velocity of the primary system, the x-axis is directed from P_1 to P_2, and the y-axis completes the right-handed basis.

II.A.2. Three-body dynamical model (CRTBP)

The equations of motion for a third-body in the CRTBP are derived from Newton's second law of motion, that is, the acceleration of a particle in the gravity field is derived from the gradient of the gravitational potential function. As expressed in the rotating frame, the EOMs are written as,

$$\ddot{\bar{\rho}} + 2\bar{\omega} \times \dot{\bar{\rho}} + \bar{\omega} \times (\bar{\omega} \times \bar{\rho}) + \dot{\bar{\omega}} \times \bar{\rho} = \frac{\partial U}{\partial \bar{\rho}} \tag{1}$$

where $\omega = n\hat{z}$ and n is constant and equal to 1 in the nondimensional unit system, $\bar{\rho} = x\hat{x} + y\hat{y} + z\hat{z}$ denotes the location of the third body in the rotating frame with respect to the primary system barycenter. Thus, under the assumptions in the CRTBP, the nondimensional EOMs are reduced to,

$$\ddot{\bar{\rho}} = [2n\dot{y} + U_x, -2n\dot{x} + U_y, U_z] \tag{2}$$

where $U(x, y, z, n) = \frac{1}{2}n^2\left(x^2 + y^2\right) + \frac{1-\mu}{d} + \frac{\mu}{r}$ is the pseudo-potential function, d and r represent the distances between the third body and the primaries P_1 and P_2, respectively. Then, the quantities U_x, U_y, and U_z represent the partial derivatives of U with respect to the nondimensional coordinates of the third body position. The EOMs are time-invariant and there is a unique known integral of the motion, labeled Jacobi constant, defined as $C = 2U - v^2$ where v denotes the magnitude of the rotating velocity vector of the third body.

II.B. Sphere-Ellipsoid Systems

A first step in increasing the complexity of the model for the primary system and, consequently, the model that describes the motion of a third body that evolves near such a system, is to consider each primary as a massive body rather than a point mass. Consider a configuration such that the primary P_1 is a constant density tri-axial ellipsoid and P_2 is a sphere.

II.B.1. Motion of the primary system

To describe the mutual motion of a pair of massive bodies, consider the Full Two-Body Problem (F2BP). Define one primary, P_1, as an ellipsoid with semi-major axes α, β, and γ, and let P_2, the second primary, be spherical.[6,11] The distance separating the two primaries, between their respective centers of mass, is denoted r. Both bodies are uniform with constant density. In general, the motion of P_2, with respect to P_1, is numerically simulated in a rotating frame (R_{P_1}) that is fixed with the ellipsoidal primary P_1 with unit vectors that are aligned along the ellipsoid semi-major axes. A second rotating frame (R_{P_2}), one that is rotating with the second primary, i.e., P_2, is also introduced, as illustrated in Figure 1. The EOMs for the mutual motion of a sphere and an ellipsoid are derived from Newton's second law of motion, as viewed by an inertial observer. To facilitate numerical exploration, a set of characteristic quantities to nondimensionalize the equations are introduced. The characteristic distance is selected as the largest ellipsoid semi-major axes α and the characteristic time is defined as the inverse of the mean orbital motion of the system at this radius, that is, $t^* = \sqrt{\alpha/G(m_1+m_2)}$. In the rotating frame that is fixed with the ellipsoid, the nondimensional translational and rotational equations of motion are written,

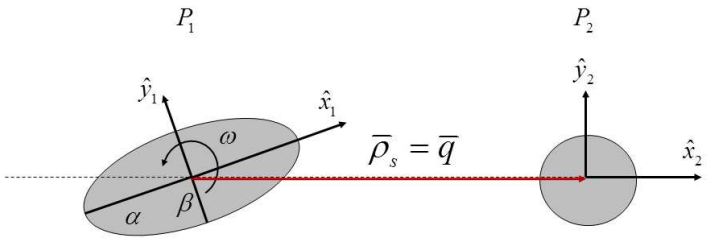

Figure 1. Sphere-ellipsoid full two-body problem geometry

$$\ddot{\bar{\rho}}_s + 2\bar{\omega}\times\dot{\bar{\rho}}_s + \bar{\omega}\times(\bar{\omega}\times\bar{\rho}_s) + \dot{\bar{\omega}}\times\bar{\rho}_s = \frac{\partial U_{e_1}}{\partial\bar{\rho}_s} \tag{3}$$

$$\bar{\bar{I}}\cdot\dot{\bar{\omega}} + \bar{\omega}\times\bar{\bar{I}}\cdot\bar{\omega} = -\mu\bar{\rho}_s\times\frac{\partial U_{e_1}}{\partial\bar{\rho}_s} \tag{4}$$

where $\bar{\rho_s} = x_s\hat{x}_1 + y_s\hat{y}_1 + z_s\hat{z}_1$ is the nondimensional position vector that denotes the location of the center of mass of the spherical primary with respect to the ellipsoid center of mass in the ellipsoid-fixed rotating frame, $\bar{\omega}$ is the angular spin rate of the ellipsoidal primary such that $\bar{\omega}$ is aligned with the inertial $\hat{Z}$ direction, $\bar{\bar{I}}$ is the inertia dyadic for the ellipsoid, and U_{e_1} represents the gravitational potential. Dots denote derivatives with respect to time as viewed by an observer in the working rotating frame, that is, R_{P_1}. It is further assumed that the two primaries move along coplanar orbits, as viewed by an inertial observer, reducing the problem to a two Degree-Of-Freedom (DOF) Hamiltonian system, labeled $\bar{\rho}_s$ and $\bar{p}$. In Hamiltonian form, these EOMs are written in the form,

$$\dot{\bar{\rho}}_s = H_{\bar{p}} \;\;;\;\; \dot{\bar{p}} = -H_{\bar{\rho}_s} \tag{5}$$

where $\bar{\rho}_s$ is the position vector that denotes the location of the sphere with respect to the ellipsoid in the R_{P_1} frame. Then, $\bar{p}$ denotes the corresponding inertial velocity vector, and H is the scalar Hamiltonian. Formulating the problem in terms of Hamiltonian variables offers the advantage of explicit expressions for the angular rate ω and its rate of change $\dot{\omega}$. The Hamiltonian for the ellipsoid-sphere system is,

$$H = \frac{1}{2}\bar{p}.\bar{p} + \frac{\mu}{2I_{zz}}\left[K - \hat{z}\cdot(\bar{\rho}_s\times\bar{p})\right]^2 - U_{e_1} \tag{6}$$

where I_{zz} is the ellipsoid moment of inertia along the inertial $\hat{Z}$ direction, K is the magnitude of the angular momentum of the system, and U_{e_1} denotes the mutual potential of the ellipsoid-sphere system, that is, computed as an elliptical integral. The simplified Hamiltonian equations of motion in Eq. 5 are numerically integrated to simulate the behavior of any given ellipsoid-sphere system.

II.B.2. Three-body dynamical model (SETBP)

The motion of a massless third body is modeled assuming that the primary system is comprised of the two massive bodies, P_1 and P_2, as illustrated in Figure 2. Note in the figure that the third particle is located relative to the ellipsoid center of mass, as viewed in the ellipsoid-fixed frame, by the position vector $\bar{\rho}_e = x_e\hat{x}_1 + y_e\hat{y}_1 + z_e\hat{z}_1$. Similar to the full two-body problem, the equations of the motion that describe the behavior of a massless particle near a primary system are derived from Newton's second law, that is, the acceleration of a particle in the gravity field is derived from the gradient of the gravitational potential function. The EOMs are,

$$\ddot{\bar{\rho}}_e + 2\bar{\omega} \times \dot{\bar{\rho}}_e + \bar{\omega} \times (\bar{\omega} \times \bar{\rho}_e) + \dot{\bar{\omega}} \times \bar{\rho}_e = \frac{\partial U_{SE}}{\partial \bar{\rho}_e} + \frac{\partial U_{e_1}}{\partial \bar{\rho}_s} \tag{7}$$

where $\bar{q}$ represents the location of the sphere center of mass and $\bar{\omega}$ is the orbital angular rate of the ellipsoidal primary P_1. The symbol U_{SE} then denotes the gravitational potential defined as $U_{SE} = \mu U_s + (1-\mu)U_{e_1}$ where U_s and U_{e_1} represent the potentials that are associated with the sphere and the ellipsoid, respectively. Since no analytical solution to the EOMs exists, the set of differential equations is numerically integrated along with the F2BP EOMs to simulate the motion of a massless third particle.

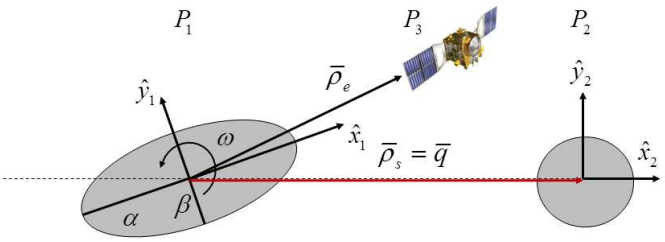

Figure 2. Three-body problem geometry under periodic F2BP

II.B.3. Synchronous systems

From the general formulation, two equilibrium primary configurations are identified: the long-axis equilibrium and the short-axis equilibrium configurations. Initially, consider the long-axis configuration, that is, a primary orientation such that the ellipsoid largest semi-major axis direction, α, is aligned with the ellipsoid-sphere direction $\hat{x}_2$. For this configuration to be maintained, both rotating frames coincide and the primaries P_1 and P_2 appear to be fixed in the rotating frame. This configuration is labeled 'synchronous'. Also true in synchronous systems, the angular velocity $\bar{\omega}$ is constant in both magnitude and direction.

II.C. Ellipsoid-Ellipsoid Systems

The complexity in the dynamical model is further increased by considering a primary system that is comprised of two rotating ellipsoids, i.e., both P_1 and P_2 are modeled as tri-axial constant density ellipsoids. Similar to the Sphere-Ellipsoid problem, the motion of the primary system is first addressed before deriving the equations that govern the motion of a third massless body near such a system.

II.C.1. Motion of the primary system

One strategy to derive the equations of the motion that describe the time evolution of such a system is to assume that the mutual orbit of the two ellipsoids is coplanar and equatorial. Then, the problem can be fully described with four degrees of freedom, q_i, one distance and three angles.[12] First, an inertially fixed frame $(\hat{e_1}, \hat{e_2}, \hat{e_3})$ is defined such that the plane spanned by $(\hat{e_1}, \hat{e_2})$ is parallel to the orbital plane of the primary

system. Then, a second frame is defined consistent with the rotating frame in the CRTBP, that is, the first base vector $\hat{s_1}$ is directed from P_1 to P_2 between the centers of mass, $\hat{s_3}$ is parallel to the angular orbital velocity of the primary system, and $\hat{s_2}$ completes the right-handed unit vector basis. Thus, the inertial and orbital frames are related through a rotation about the inertial direction $\hat{e_3} = \hat{s_3}$ by the angle θ. Also, both ellipsoids are assumed to be rotating about the third inertial direction, $\hat{e_3}$, such that the orientation between the body fixed-frame $(\hat{x_i}, \hat{y_i}, \hat{z_i})$ that is associated with the primary i and the orbital frame is fully described by the angle ϕ_i. Consequently, $\hat{e_3} = \hat{z_1} = \hat{z_2}$. Finally, the distance r denotes the separation between the two primary bodies, as illustrated in Figure 3. Then, the Lagrangian equations of the motion for the primary system, of the form $d\left(\partial L/\partial \dot{q_i}\right)/dt = \partial L/\partial q_i$, are derived as follows,

$$\ddot{r} = \dot{\theta} r - \frac{1}{m} V_r \tag{8}$$

$$\ddot{\phi_1} = -\left(1 + \frac{mr^2}{I_{1_z}}\right) \frac{1}{mr^2} V_{\phi 1} - \frac{1}{mr^2} V_{\phi 2} + 2\frac{\dot{r}\dot{\theta}}{r} \tag{9}$$

$$\ddot{\phi_2} = -\left(1 + \frac{mr^2}{I_{2_z}}\right) \frac{1}{mr^2} V_{\phi 2} - \frac{1}{mr^2} V_{\phi 1} + 2\frac{\dot{r}\dot{\theta}}{r} \tag{10}$$

$$\ddot{\theta} = \frac{1}{mr^2} \left(V_{\phi 1} + V_{\phi 2}\right) - 2\frac{\dot{r}\dot{\theta}}{r} \tag{11}$$

where m denotes the reduced mass of the primary system defined as $m = m_1 m_2/(m_1 + m_2)$. Then, $V_r = \partial V/\partial r$, $V_{\phi 1} = \partial V/\partial \phi_1$, and $V_{\phi 2} = \partial V/\partial \phi_2$ and V is the potential energy of the system defined as,

$$\begin{aligned} V(r, \phi_1, \phi 2) = -\frac{G m_1 m_2}{r} \Bigg\{ 1 + \frac{1}{2r^2} \Bigg[Tr(\bar{\bar{I}}_1) + Tr(\bar{\bar{I}}_2) - \frac{3}{2} \left(I_{1_x} + I_{1_y}\right. \\ \left. - \cos 2\phi_1 \left(I_{1_y} - I_{1_x}\right) + I_{2_x} + I_{2_y} - \cos 2\phi_2 \left(I_{2_y} - I_{2_x}\right)\right)\Bigg]\Bigg\} \end{aligned} \tag{12}$$

where G is the universal gravitational constant and $\bar{\bar{I}}_1$ and $\bar{\bar{I}}_2$ represent the inertia dyadics associated with P_1 and P_2, respectively, such that $\bar{\bar{I}}_i = diag\left[I_{i_x}, I_{i_y}, I_{i_z}\right], i = 1, 2$.

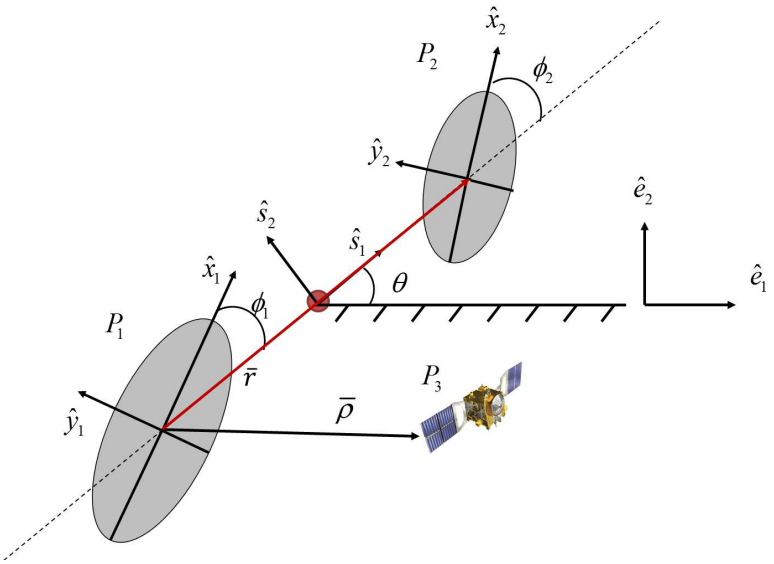

Figure 3. Ellipsoid-ellipsoid full two-body problem and three-body problem geometry

II.C.2. Three-body dynamical model (EETBP)

The motion of a massless third body is modeled assuming that the primary system is comprised of the two massive ellipsoids, P_1 and P_2, as illustrated in Figure 3. Note in the figure that the third particle is located

relative to the first primary, P_1, center of mass, as viewed in the inertially-fixed frame, by the position vector $\bar{\rho} = x\hat{e}_1 + y\hat{e}_2 + z\hat{e}_3$. Similar to the full two-body problem, the equations of the motion that describe the behavior of a massless particle near a primary system are derived from Newton's second law. Expressed with respect to the inertial frame, the EOMs are,

$$\ddot{\bar{\rho}} = \frac{\partial U_{EE}}{\partial \bar{\rho}} \tag{13}$$

where the symbol U_{EE} then denotes the gravitational potential defined as $U_{EE} = (1-\mu)U_{e_1} + \mu U_{e_2}$ where U_{e_1} and U_{e_2} represent the potential that is associated with P_1 and P_2, respectively. Similar to the CRTBP and SETBP, where no analytical solution to the EOMs exists, the set of differential equations is also numerically integrated along with the F2BP EOMs to simulate the motion of a massless third particle.

II.C.3. Synchronous systems

Similar to the sphere-ellipsoid model, a synchronous configuration is identified such that the two ellipsoids largest semi-major axis directions, α_1 and α_2, are each aligned with the ellipsoid-ellipsoid direction $\hat{s}_1$. For this configuration to be maintained, both rotating frames coincide and the primaries P_1 and P_2 appear to be fixed in the rotating frame. Also true in synchronous systems, the angular velocity $\dot{\theta}$ is constant in magnitude.

II.D. Polyhedron-Polyhedron Systems

An alternate approach to the spherical or ellipsoidal shape model for the representation of the primaries in a given system is a model that constructs each body as a constant density polyhedron. There is no restriction on the geometric complexity in the polyhedron model; as a consequence, the relative orbital motion and the attitude orientation of the two bodies are coupled. Note that polyhedron shape models for each primary can be constructed with symmetry properties that would yield equilibria primary configurations, or synchronous configurations. However, since such scenarios are captured by the simplified dynamical models, SETBP and EETBP, and, thus, the focus is on systems with very irregular, hence, asymmetric, shape models.

II.D.1. Motion of the primary system

The coupled relative motion of a primary system such that each massive body is an arbitrarily-shaped but constant density polyhedron can be numerically integrated. One approach exploits a semi-implicit Lie Group Variational Integrator (LGVI) and the discretized equations of the motion for the full two-body problem as expressed in a frame that is fixed with and centered at the primary P_1.[8,13] The EOMs are coupled and include both the relative orbital motion as well as the attitude of the two bodies as time evolves. As part of the integration process, the mutual forces and moments, that is, the resultant force and moment that each body exerts on one another, must be evaluated. There is no known exact method to compute these quantities for a pair of arbitrary polyhedra, rather the algorithm relies on an infinite series expansions of the gravitational potential function. Then, the force and moment terms are computed as the derivatives of the approximated potential function with respect to the relative position vector and the relative attitude matrix, respectively.[14,15] Also, the numerical integration is very computationally expensive and a trade-off between the resolution of the discretization for each shape model and the number of terms to include in the series expansion for the gravitational potential approximation is necessary to achieve reasonable computation times. For this analysis, a C++ program that leverages Message Passing Interface (MPI) is employed to perform the integration of the relative motion for a given binary system. Simulations are performed on Purdue University's cluster Coates using up to 2800 cores (350 nodes).

II.D.2. Three-body dynamical model (PPTBP)

The motion of a massless third body is modeled assuming that the primary system is comprised of the two constant density polyhedra, P_1 and P_2, where the relative motion of the primary system is pre-computed. Note that the third particle is located relative to the primary P_1 center of mass, as viewed in the inertially-fixed P_1-centered frame. However, the problem can be similarly formulated for either primary as the central body. The equations of motion that describe the behavior of a massless particle near such a primary system are similar to the ellipsoid-ellipsoid problem, as expressed with respect to the inertial frame in Eq. 13

where the symbol U_{EE} is replaced with U_{PP}. The symbol U_{PP} now denotes the gravitational potential defined as $U_{PP} = (1-\mu)U_{p_1} + \mu U_{p_2}$ where U_{p_1} and U_{p_2} represent the potential that is associated with the polyhedra P_1 and P_2, respectively. In contrast to the motion of the primary system, where the mutual gravitational potential is expressed in terms of an infinite series, the gravitational potential that is exerted on the massless third body by each polyhedron can be computed independently. For the gravitational potential, and consequently the gravitational force, exerted by a single constant density polyhedron onto a massless particle, there exists an exact closed-form solution.[16,17] Thus, the gravitational potential is exact for a given shape and density. The resolution of the calculated field depends directly on the level of discretization selected for a particular shape. However, the polyhedron is still an approximation for the actual shape of the body and the accuracy of the gravity field is consistent with its shape determination.

III. Bounded Motion in Synchronous Systems

Within the context of exploring third-body trajectories in the vicinity of two small irregular bodies, that is, a problem where investigating the motion in close proximity to the primaries is necessary, two spherical primaries may not, in general, be a reasonable assumption. This more specific problem motivates the introduction of a dynamical model that incorporates more complexity in the primary system model. In addition to the CRTBP, consider the synchronous Sphere-Ellipsoid Three-Body Problem (SETBP) and the synchronous Ellipsoid-Ellipsoid Three-Body Problem (EETBP). With similar equations of motion, both models possess attributes similar to those in the CRTBP. In particular, while no analytical solution for the motion of the particle is available, the EOMs are time-invariant and periodic solutions exist.

III.A. Periodic Orbits in Synchronous Systems

To explore the dynamical behavior of a third body within the vicinity of two primaries, periodic orbits are of special interest. A multi-phase technique based on differential corrections is employed to compute a trajectory that is periodic in the nonlinear regime given some initial guess. The same algorithm is used to produce such trajectories for any of the simplified dynamical models, that is, CRTBP, SETBP, or EETBP. A trajectory is labeled periodic if there exists no discontinuity between two six-dimensional states along the path that exceeds a prescribed tolerance, typically 10^{-11} nondimensional units.

III.A.1. Libration Point periodic Orbits. (LPO)

Most common families of periodic orbits within this regime are labeled libration point orbits and a preliminary exploration of the dynamical structures typically originates near any equilibrium solutions. The first-order variational equations of motion are employed to generate an initial guess in the vicinity of a given equilibrium point. In this problem, there are, in general, five equilibrium points and the equilibrium locations evolve as a function of the system mass ratio and the ellipsoid semi-major axes distances of each primary.[7] First, the planar Lyapunov families corresponding to the equivalent collinear Lagrange points are computed for a sample system. Employing a continuation strategy, additional families of more complex orbits that include three-dimensional trajectories are also computed, as illustrated in Figure 4 for a sample ellipsoid-sphere system with one elongated primary. In this plot are displayed Lyapunov, halo, and axial families of periodic orbits associated with each of the three collinear points. Although not illustrated in this figure, similar families of orbits can also be constructed in the vicinity of the two equilateral points. Although these families of orbits may or may not offer options for any direct application in design or analysis scenarios, these trajectories are most useful in constructing even more complex trajectories.

III.A.2. Resonant periodic orbits.

Other families of periodic orbits within this regime include trajectories that are labeled resonant orbits. The classical restricted two-body problem is leveraged to generate an initial guess to produce a periodic orbit in the three-body regime via a corrections strategy and/or continuation. Within the context of the restricted two-body problem, consider two bodies, A and B, that orbit a primary body. The primary body is massive while body A and B are assumed massless, consistent with the restricted two-body problem model. Body B is defined to be in $p:q$ resonance with body A if it completes p orbits with respect to the primary in the same time interval in which body A achieves exactly q orbits.[18] In this definition, p and q are two positive

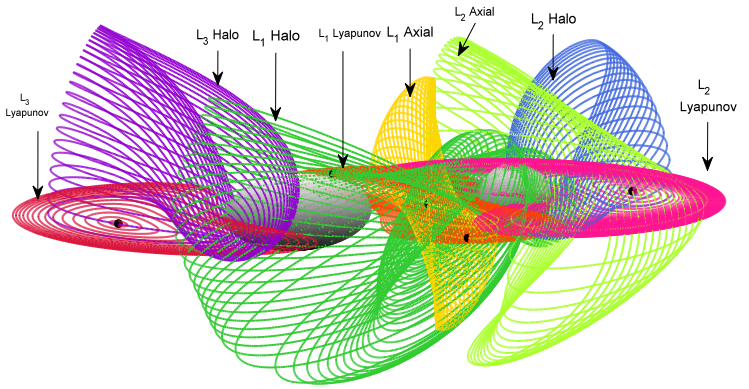

Figure 4. Libration point Periodic Orbits (LPO): ellipsoid axes ratios $\beta = \gamma = 0.5$ - primary mass ratio $\mu = 0.3$ - primary distance $r = 3$

integers where p is associated with body B and q refers to the period of body A. For instance, a spacecraft moves in a $1 : 2$ resonance with the Moon if it completes one revolution around Earth in the same time that the Moon completes two periods. In this analysis, the primary is the primary P_1, body A is the second primary, P_2, and the third body, B, is a spacecraft. Using the restricted two-body problem to produce an initial guess for a resonant orbit given some resonant ratio $p : q$, an orbit that is periodic and possesses approximately the initial resonant ratio in the three-body regime is computed. Employing a continuation method, a family of resonant orbits, or, a set of orbits that share some common characteristics, is computed. Also, exploiting bifurcations within the planar resonant family, other families with the same resonance ratio that include symmetric or asymmetric three-dimensional trajectories can be generated. First, families of planar resonant orbits for various $p : q$ ratios are computed for a sample point mass, ellipsoid-sphere, and ellipsoid-ellipsoid system. In Figure 5 is illustrated selected families of planar resonant orbits as computed for a sample ellipsoid-ellipsoid system with an elongated primary with largest equatorial P_1 radius of 5 km, ellipsoid axes ratios $\beta = \gamma = 0.5$, primary mass ratio $\mu = 0.2$, and primary distance $r = 6$. While the various families exhibit orbits with very different shapes and sizes, all offer one or more close encounters with at least one primary body. Then, in Figure 6 is illustrated selected sample three-dimensional families of symmetric and asymetric resonant orbits computed for a sample ellipsoid-sphere system with an elongated primary with largest equatorial P_1 radius of 5 km, ellipsoid axes ratios $\beta = \gamma = 0.5$, primary mass ratio $\mu = 0.2$, and primary distance $r = 6$. Similar to the libration point orbits, these families of orbits may or may not offer options for any direct application in design scenarios, however, these trajectories are also useful in constructing even more complex trajectories.

III.A.3. Low Prograde Orbits (LoPO) and Distant Retrograde Orbits (DRO)

Periodic orbits labeled Distant Retrograde Orbits (DRO) and Low Prograde Orbits (LoPO) are also of special interest as these families feature numerous stable orbits. The DROs are, in fact, 1:1 resonant orbits. Planar LoPOs are also centered at one primary, P_1 or P_2. Exploiting bifurcations within the planar families, and employing a continuation technique, a three-dimensional family that branches from the planar family is also computed, as illustrated in Figure 7 for a sample sphere-sphere system with P_1 radius of 5 km. As clearly apparent in the figure, the orbits in the three-dimensional families allow regular close-range proximity of a third-body with respect to either primary. In addition, the three-dimensional aspect of the trajectories offers extensive coverage of the surface of the attractive primary.

III.A.4. Stability analysis

A key factor to assess the suitability of a trajectory for a given application is often its stability. Significant information concerning the stability of a particular solution is available from the first-order variational equations relative to a reference. For a periodic orbit, the monodromy matrix, M, is defined as the state transition matrix evaluated after exactly one orbital revolution along the reference path, that is, $M =$

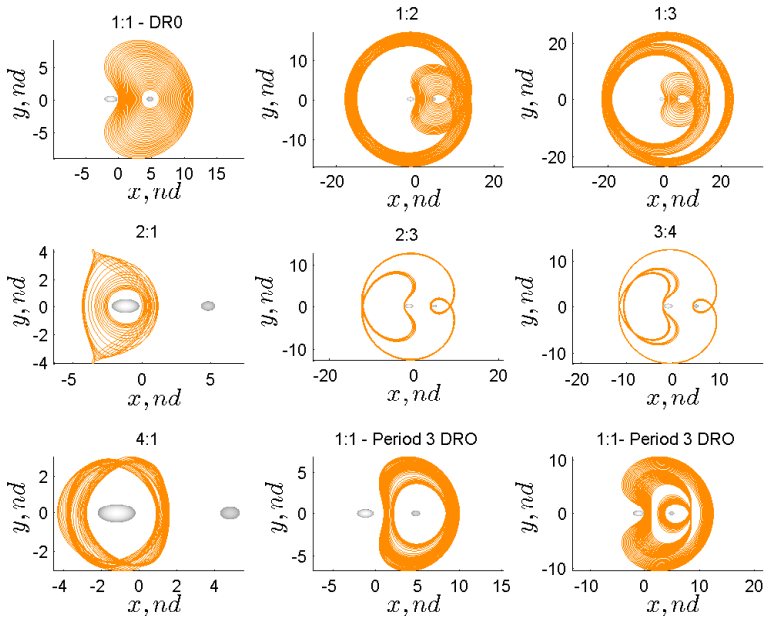

Figure 5. Sample families of planar resonant orbits: ellipsoid axes ratios $\beta_1 = \gamma_1 = 0.5$ - $\beta_2 = \gamma_2 = 0.65$ - primary mass ratio $\mu = 0.2$ - primary distance $r = 6$

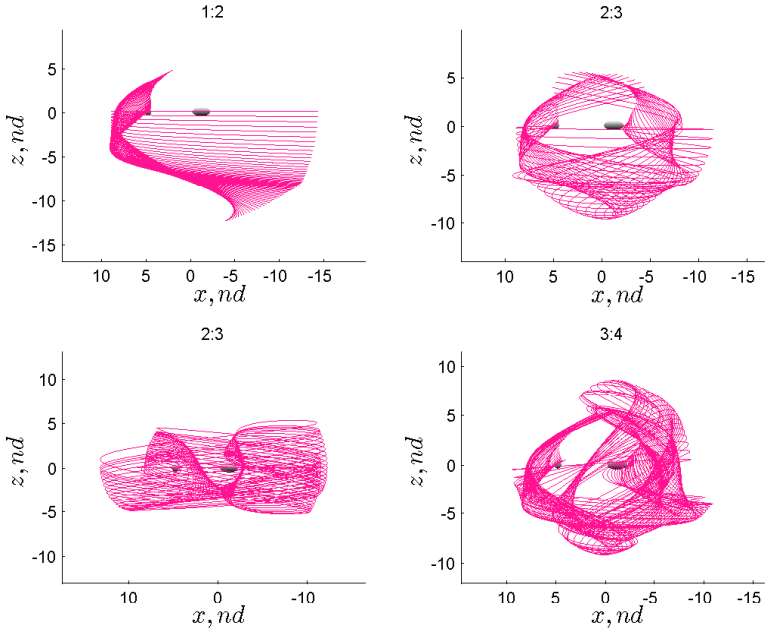

Figure 6. Sample families of 3D resonant orbits: : ellipsoid axes ratios $\beta_1 = \gamma_1 = 0.5$ - primary mass ratio $\mu = 0.2$ - primary distance $r = 6$

$\Phi(t + P, t)$. The eigenvalues of the monodromy matrix are then computed for each orbit of interest. The dynamical model for the motion of a particle in this problem represents a three degree-of-freedom Hamiltonian system. Consequently, the monodromy matrix admits six eigenvalues that occur in reciprocal and complex conjugate pairs,[19] where two are always equal to unity.[20] Define the stability index, ν, as the average of each reciprocal pair of eigenvalues, that is, $\nu = \frac{1}{2}(\lambda + \lambda^*)$ for the reciprocal pair $(\lambda + \lambda^*)$, where ν is a numerical quantity to assess the stability of a given solution. For a periodic orbit, one pair of eigenvalues is always unity, thus, the four remaining multipliers define two stability indexes. A first horizontal index is associated with stability in the plane of the orbit, $\nu = \nu_h$, and a vertical index that corresponds to out-of-plane stability, that is, $\nu = \nu_v$. For values of ν less than 1, the orbit is defined as stable, and alternately, an orbit is labeled

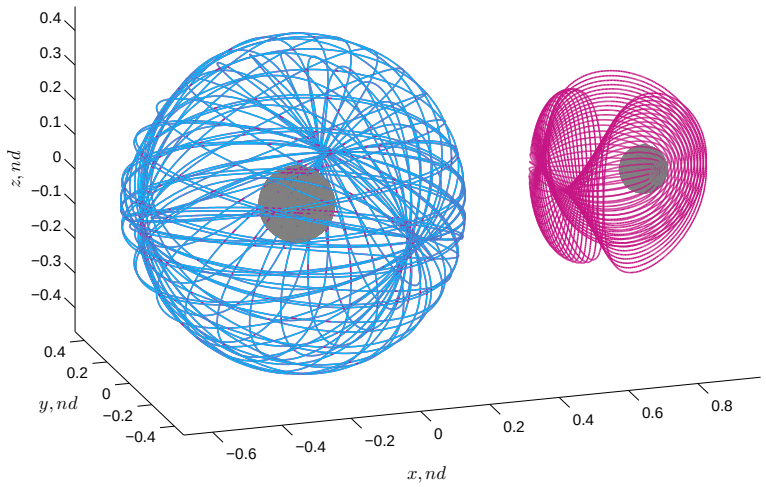

Figure 7. P_1 **and** P_2 **centered 3D LoPO families: primary radius = 5 km - primary mass ratio** $\mu = 0.2$ **- primary distance** $r = 6$

unstable for values of ν greater than 1. The orbit is unstable if either index exceeds 1. Finally, a graphical approach is proposed to quickly assess the stability properties of a given solution as a part of a family of periodic orbits without losing visibility concerning the overall behavior of the family of interest. Specifically, consider the maximum stability index defined as $\nu_{max} = max\left\{|\nu_v|, |\nu_h|\right\}$. Then, for values of ν_{max} less than 1, the orbit is defined as stable, otherwise it is unstable. However, using such a representation, the form of the instability is not clear.

First, consider selected families of libration point orbits. In Figure 8 is illustrated the maximum stability index as a function of the abscisse of the initial point of individual trajectories, scaled by the primary separation distance, within a given family of libration point orbits. Each of the families is computed for a sphere-sphere, sphere-ellipsoid, and ellipsoid-ellipsoid sample system to highlight the effect of the shape of the primary bodies onto the dynamical behavior of a third body in the vicinity of such a primary system. In the CRTBP, the selected families of orbits in this figure, that is, L_1 and L_3 Lyapunov, L_1, L_2, and L_3 halo, and L_3 vertical, all but the L_1 halo family exhibit some stable members, as depicted by the maximum stability index line achieving values less than one for some trajectories. The families that are computed for the sphere-ellipsoid system exhibit the same behavior in most instances, with the exception of the L_3 Lyapunov and halo families where no stable orbits exist. Note that, for the models that incorporate a massive body model in the primary system, i.e., an ellipsoid, as opposed to a point mass, the families are only computed until a trajectory first collides with one of the primaries. Further differences appear when considering the families computed for the ellipsoid-ellipsoid system. In particular, the ellipsoidal shape of the second primary has a significant impact on the behavior of the L_1 and L_2 halo orbits as these families feature orbits with very close approaches to P_2. Consequently, stable orbits exist in the L_1 halo family while only unstable trajectories are apparent for the sphere-sphere and sphere-ellipsoid families. Alternatively, while numerous stable orbits belong to the L_2 halo families for the sphere-sphere and sphere-ellipsoid systems, only very few stable members exist for the ellipsoid-ellipsoid families. Overall, stable periodic orbits in close proximity of one or two primaries apparently exist even when considering dynamical models that incorporate non-spherical primary shape models. In Figure 9 is illustrated stable members from the families computed for the ellipsoid-ellipsoid model. A variety of shape and size is available and such trajectories may suggest interesting applications for mission scenarios that involve close observations of one or both primary bodies.

A similar analysis for some selected planar resonant orbits illustrated in Section III.A.2. The stability properties associated with these families are depicted in Figure 10. Similar to the libration point families, the overall stability behavior of the members within a given family is similar between the three dynamical models examined. However, differences do exist and such discrepancies are emphasized for trajectories that include very close passages with one of the primary bodies. Again, stable periodic orbits that involve close proximity to one or two primaries exist even when employing dynamical models that incorporate non-spherical primary shape models. Finally, most three-dimensional resonant orbits are unstable as computed

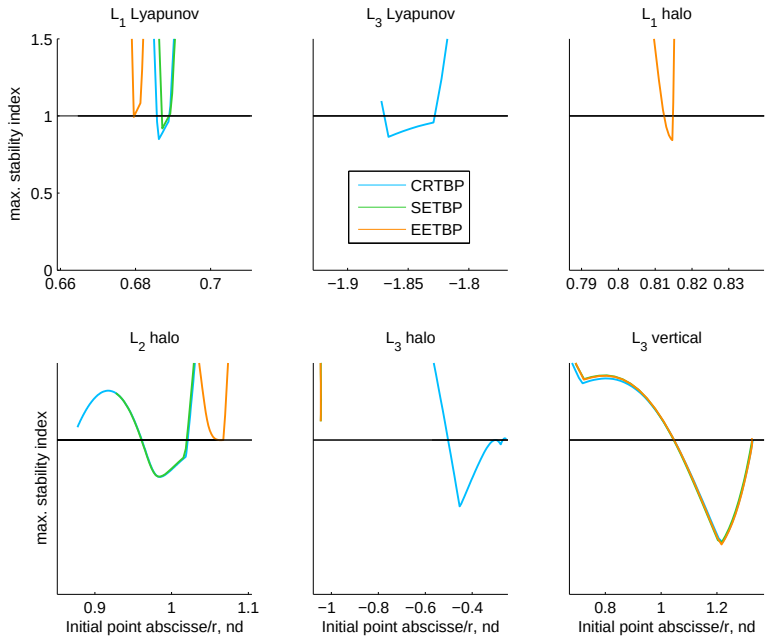

Figure 8. Maximum stability index for selected libration point families in the CRTBP, SETBP, and EETBP

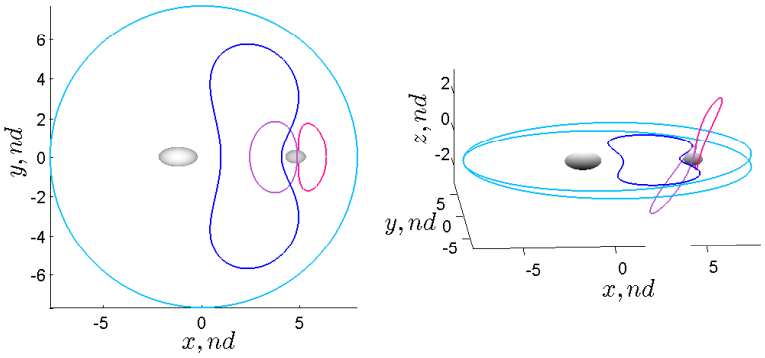

Figure 9. Sample stable libration point orbits in the EETBP

for the set of parameters in this analysis. Finally, the low prograde orbits that surround P_1 reflect another family of periodic orbits that feature close approaches to a primary. This family also possesses numerous members that are defined as stable, as illustrated for a sample sphere-sphere system in Figure 11. Note that the stability index is now plotted as a function of the period of the trajectories. The shortest period orbit corresponds to the bifurcation from the LoPO planar family. Recall that any member with a maximum stability index value less than one is labeled as stable. In the figure, two regions with trajectories that satisfy the stability criterion are apparent. Then, the two cusps where the maximum stability index reaches a local minimum correspond to trajectories such that the combination of both stability indexes yield a minimum, in a sense, these orbits are the most stable members in the family to some arbitrary perturbation.

III.B. Continuation

The specific existence, shape, and other relevant characteristics, e.g., stability, of an individual orbit or a family of trajectories depends on the physical and dynamical properties of the primary system. Specifically, the mass ratio of the system, the primary separation distance, and the shape of the individual primary bodies are some of the most influential parameters. Within the context of preliminary mission design, it is impractical to produce an extensive catalog of the infinite number of potential periodic orbits for sample

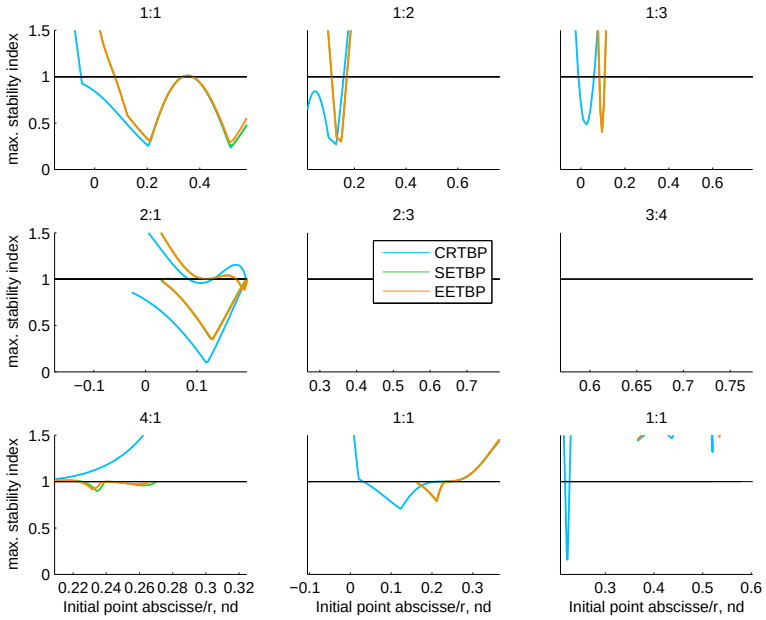

Figure 10. Maximum stability index for selected families of resonant planar orbits

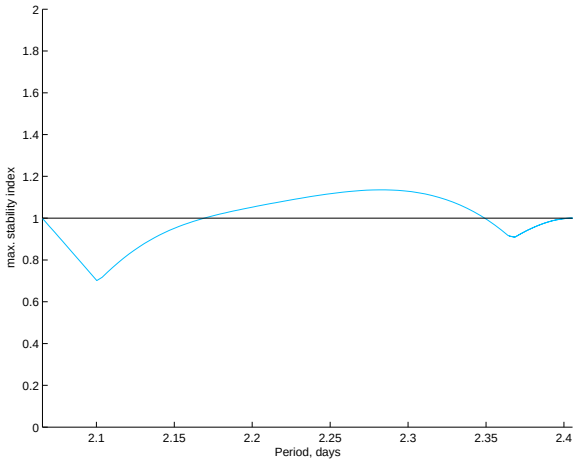

Figure 11. Maximum stability index for 3D P_1-centered LoPO family

primary system models that cover the entire design space. However, assume a pre-computed catalog for a few sample systems, one that is reasonably representative of the overall behavior. Then, an automated process that exploits natural parameter continuation is employed to produce a specific trajectory for any desired primary system model. As an example, a three-dimensional 2:3 symmetric resonant orbit is computed for the known binary system 1999 KW4; the trajectory is generated from a 2:3 symmetric resonant orbit initially computed in the CRTBP for a sample system. In Table 1 are summarized the characteristics that are associated with the sample system and the 1999 KW4 model. The initial and continued trajectories are illustrated in Figure 12. Although the mass ratio corresponding to the two primary models is very different, the continued trajectory retains the same overall characteristics as viewed in configuration space.

III.C. Tours

Within the context of exploring the regions near the primary bodies, isolated periodic orbits may or may not be suited for direct application in mission scenarios, however, such periodic orbits can be used to construct a trajectory that satisfies some desired characteristics. The goal is an automated strategy to construct a nearby

Table 1. Characteristic quantities associated with the sample system and the 1999 KW4 model

	μ	r	β_1	γ_1	β_2	γ_2
sample system	0.2	6	1	1	1	1
1999 KW4	0.0541	3.64	1	0.845	0.8109	0.6112

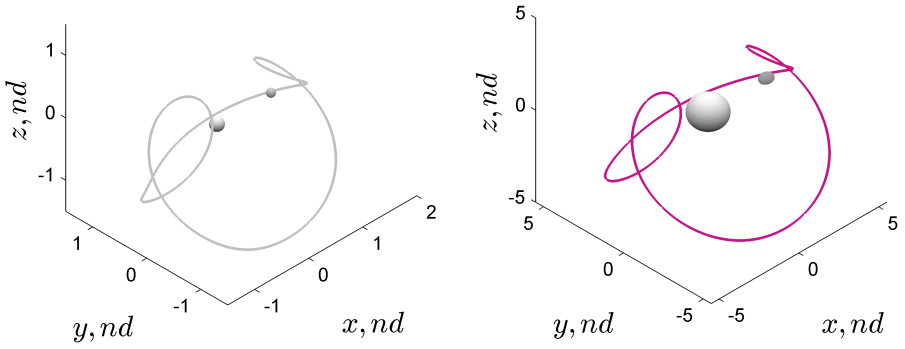

Figure 12. Sample 2:3 symmetric resonant orbit for the sample sphere-sphere system (left) and 1999 KW4 (right) computed using continuation

sequence of arcs in such systems. In an initial effort, a sample trajectory is computed for demonstration purpose. While the path is, in fact, too complex and risky to be used as a baseline solution for flight, it does, however, demonstrate that the capability of the proposed algorithm.

III.C.1. Algorithm

In preparation for future tour design algorithms, a first step is to understand how pathways in the vicinity of a binary system of irregular bodies can be exploited to construct a path with some desirable properties. The objective is an automated algorithm that leverages pre-computed periodic orbits to construct a continuous trajectory that exhibits some pre-specified characteristics. From a user-defined chain of periodic orbits, the task is the construction of a trajectory that travels between the specified orbits. The strategy is comprised of four tasks (i) Computation of transfer arcs between user-selected periodic orbits that are pre-computed. Originating from the first prescribed orbit in the chain, an arc that links one orbit to the next is constructed from the stable and unstable manifolds that are associated with two orbits that are to be linked, if such manifolds exist. If one of the two orbits is stable, the manifolds that are associated with the other orbit are solely employed to construct a direct transfer into the stable orbit. (ii) A number of user-defined revolutions of each selected periodic orbits are 'stacked' to anchor the correction process. (iii) Concatenation of the transfer arcs and periodic orbit revolutions into an initial discontinuous trajectory yields an initial guess. (iv) A continuous trajectory is then constructed from the initial guess in a differential corrections algorithm. To facilitate the corrections process and also to accommodate the differences in energy level between the selected periodic orbits, impulsive maneuvers are allowed at the nodes between a transfer arc and a periodic orbit and between two the manifold arcs that constitute one transfer arc.

III.C.2. Application

Consider a sample sphere-sphere system. In this application, three distinct periodic orbits are chained together to produce a trajectory that tours the primary system. Initially, an unstable 2:3 symmetric three-dimensional resonant orbit is selected as the departure orbit, and is periodic. Then, the construction scheme produces a first transfer arc to a three-dimensional unstable P_2 centered low prograde orbit, followed by a second transfer segment to a stable 3D P_1 centered low prograde orbit. Finally, a last arc is computed to return to the initial resonant orbit that evolves around the primary system. To allow more time for potential observations of each primary body, one revolution around each periodic orbit might be incorporated into the initial discontinuous trajectory. In Figure 13 is illustrated the resulting initial guess projected onto the

(x, y) plane where each colored segment represents a different transfer arc. The initial guess is then corrected to produce a trajectory continuous both in position and velocity. To ensure velocity continuity, impulsive maneuvers are allowed at the nodes between the various segments that constitute the initial guess. Although some maneuvers may be reduced or entirely eliminated through iterative corrections, because the energy level of the orbits selected in this application are not equal, some maneuvers are required. Without attempting to reduce or remove any maneuvers, the thrust events as computed by the algorithm are summarized in Table 2 and the total required thrust is $|\Delta V| = 1.93$ m/s. Note that time is referenced with respect to the initial epoch t_0=0. Also, the approximate time of flight of each segment appears in Table 3.

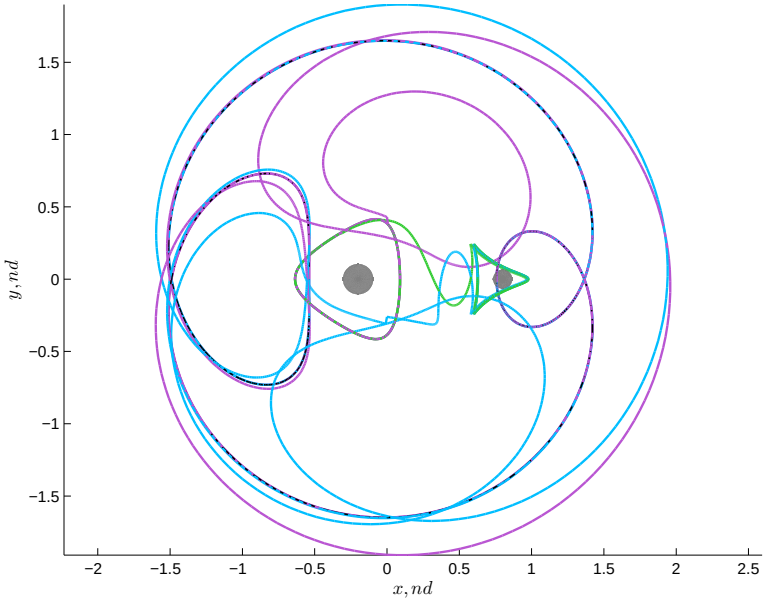

Figure 13. Initial guess from tour algorithm projected onto the (x, y) plane

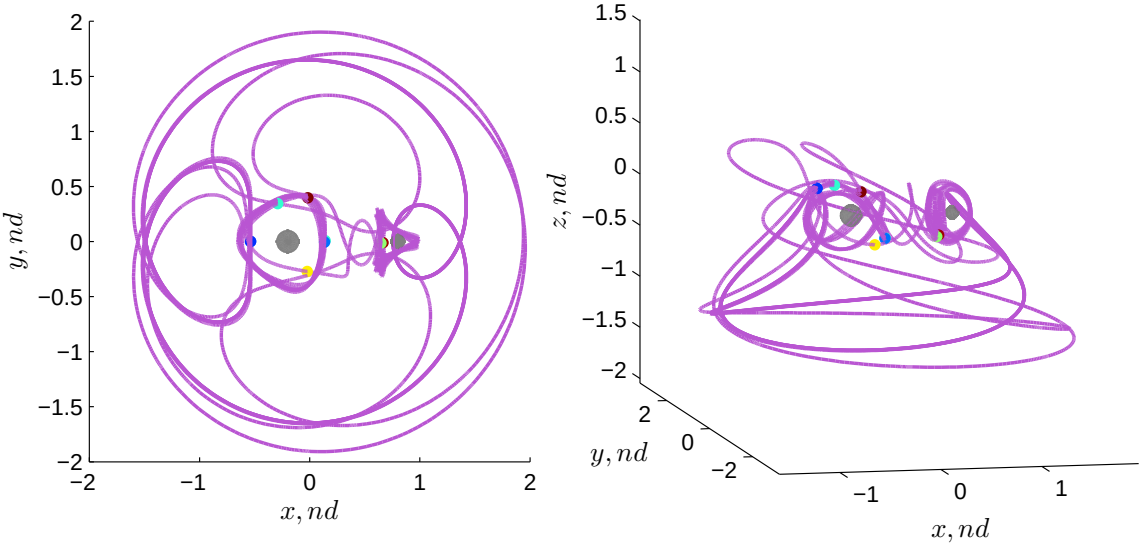

Figure 14. Converged trajectory from tour algorithm

An initial assessment of the viability of the produced trajectory is performed. The altitude of the third body with respect to each primary is evaluated as a function of time along the path. While low altitude phases are desired for observation campaigns, such trajectory segments are also the most demanding in terms of spacecraft operations. Realistically, the time frame in such systems is very fast, and there is no time for orbit determination and correction maneuvers between primary encounters. Within this context,

Table 2. Maneuver history for tour

Time (d)	5.7	17.9	20.9	22.2	27.3	29	31.2	33.6	50.8
$\|\Delta V\|$ (m/s)	0.01	0.29	0.22	0.49	0.15	0.16	0.04	0.52	0.0009

Table 3. Time of flight for individual arcs in tour

	Departure orbit	Transfer 1	P_2 LoPO	Transfer 2	P_1 LoPO	Transfer 3
Time of flight (d)	5.7	15	2	5.7	2	19.5

autonomous guidance is required. In Figure 15 is illustrated the altitude of the third body with respect to P_1 and P_2 as a function of time, where color, from blue to red, also depicts time evolution and is matched on the left-hand figure that represents the trajectory in configuration space. The altitude is reported in terms of primary radii and the black horizontal line on the altitude plots represents 1 radii, that is, a third-body altitude of 1 body radii above the spherical primary body surface. For this particular tour, the lowest altitude with respect to P_1 is approximately equal to a few body radii while it is reduced to just above 1 radii with respect to P_2. Finally, given a converged path in a sphere-sphere system and using the continuation algorithm introduced in Section III.B, a trajectory that exhibits the same characteristics is computed for an ellipsoid-ellipsoid system employing the pre-computed result from the sphere-sphere system as initial solution. The trajectory that is produced through this process appears in Figure 16 and it is apparent that the path is similar to the initial sphere-sphere solution without repeating the entire design process.

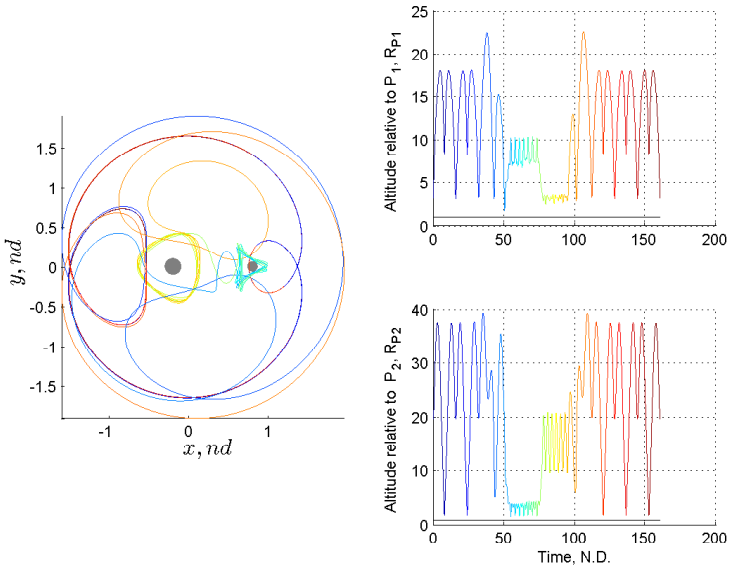

Figure 15. Altitude analysis

IV. Bounded Motion in Higher-Fidelity Dynamical Models

The simplified models that are developed in this analysis to construct complex trajectories retain some interesting system dynamical properties, such as periodicity. However, although the complexity in the primary system model is gradually increased with bodies modeled as ellipsoids rather than point masses, these models are still an idealized representation of an actual system of small bodies. An alternative approach to the ellipsoid-ellipsoid or sphere-ellipsoid models is based on modeling the primary bodies as geometric polyhedra. Such a methodology allows the representation of the actual shape of the body with a higher accuracy and, thus, enhances the fidelity. Trajectories computed from one of the simplified models can

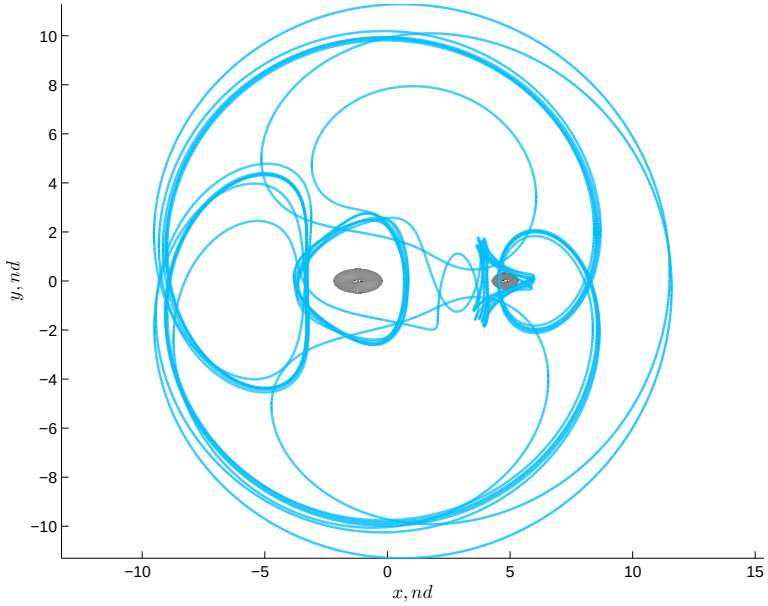

Figure 16. Converged tour for ellipsoid-ellipsoid system

be used as an initial guess for the higher fidelity model. However, periodicity no longer exists and such a dynamical model is not well-suited for extensive analysis, but it is useful to assess the robustness, stability, or feasibility of a given solution under more realistic simulation conditions.

IV.A. Primary System Model: 1999 KW4

IV.A.1. Primary shape model

In an initial investigation into the transition between the idealized dynamical models exploited thus far and a higher fidelity representation, consider the well-known Near Earth Asteroid (NEA) 1999 KW4. A medium resolution polyhedron shape model is illustrated in Figure 17 for the primary and secondary component of the KW4 binary asteroid. This shape model is derived from the full resolution model constructed in Ostro et al.[21] Also, some representative physical parameters for each body are summarized in Table 4. The primary exhibits the characteristic 'walnut' shape while the secondary, much smaller in size, is a very oblate and significantly elongated body.

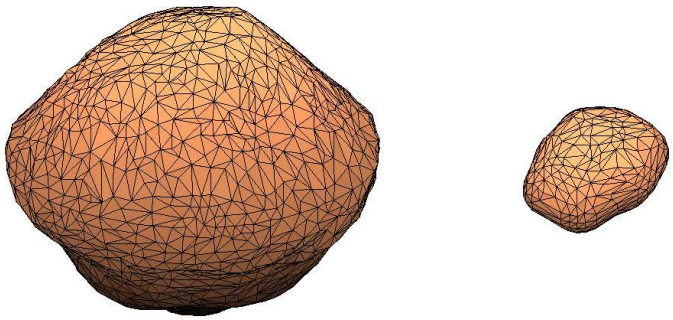

Figure 17. 1999 KW4 shape model: primary (left) and secondary (right)

Table 4. 1999 KW4 shape model

	A_X (km)	A_Y (km)	A_Z (km)	density (kg m^{-3})	rotation period (hr)
Primary	1.53	1.49	1.35	1970	2.76
Secondary	0.57	0.46	0.35	2810	17.42

IV.A.2. Primary motion simulation

The irregular shape of the two bodies directly affects the relative motion of the two primaries; the fully coupled motion of the two-body system is modeled and numerically integrated, as outlined in Section II.D.1. The initial orbital conditions and configuration for such a simulation are summarized in Table 5 for the orbital motion, in terms of semi-major axis and eccentricity, and the initial orientation of both bodies. The angles ψ_i, θ_i, and ϕ_i correspond to the Euler angles for a $3-1-3$ sequence and $i = 1, 2$ for the primary and secondary, respectively. The mutual motion, both orbital and rotational, is numerically integrated for approximately 15 revolutions of the primary system. Recall that the computation of the mutual force and torque one body exerts on the other at each time step during the numerical integration process relies on an infinite series expansion of the gravitational potential. In this simulation, only the first five terms in this series are retained, that is, four orders beyond the point mass solution. Selected results from this simulation appear in Figure 18. As expected, the irregular shape of the body directly impacts the mutual orbital motion, as clearly illustrated by the oscillating semi-major axis and eccentricity as time evolves; also, it is directly apparent in the primary-centered inertial view of the trajectory. Although, not presented here, the attitude of each body is also affected by the mutually irregular shape. For this problem, energy and angular momentum are conserved, however, it is sometimes challenging to achieve conservation of these quantities, to some tolerance, during the numerical integration process over long time intervals. In this analysis, the symplectic algorithm selected allows energy and angular moment to be conserved within reasonable and bounded values throughout the simulation.

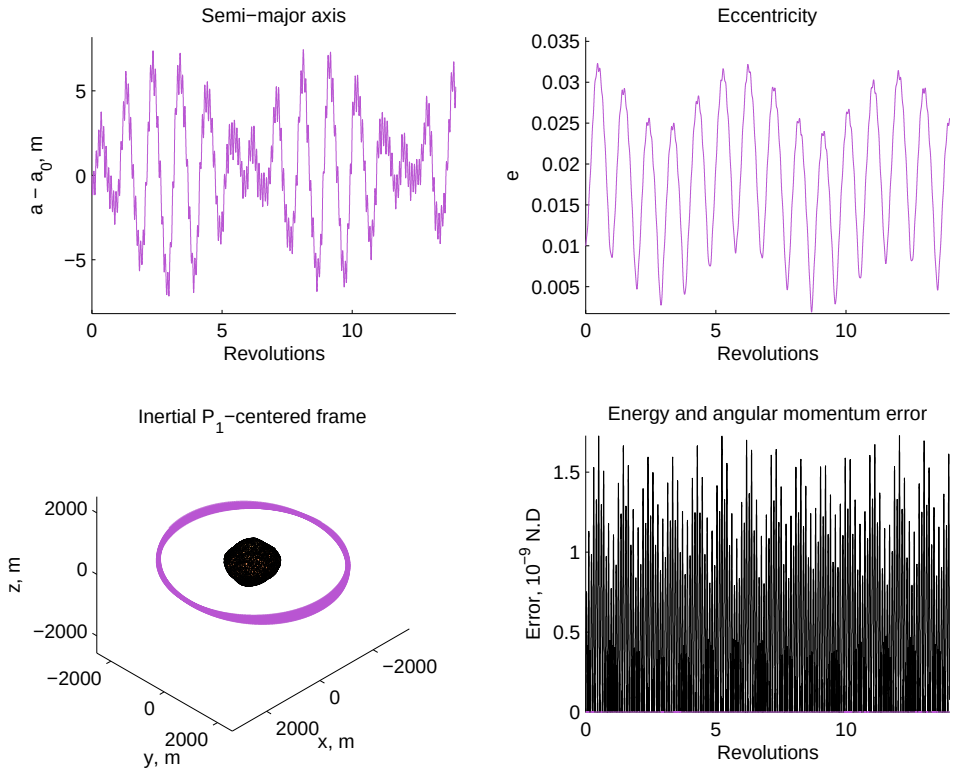

Figure 18. 1999 KW4 simulation

Table 5. 1999 KW4 initial conditions

a (km)	e	ψ_1 (deg)	θ_1 (deg)	ϕ_1 (deg)	ψ_2 (deg)	θ_2 (deg)	ϕ_2 (deg)
2.54	0.01	27.04	10	-83.93	0	0	180

IV.B. Sample Third-Body Bounded Trajectories

In an initial assessment of the robustness, stability, or feasibility of a given solution under more realistic simulation conditions, selected orbits that are pre-computed with an idealized model are employed as initial guesses in a differential corrections algorithm to produce bounded trajectories that retain similar characteristics. The third-body motion is numerically integrated based upon the relative motion of the primary system and the shape of each body. In Figures 19-21 are illustrated selected Lyapunov, halo, and axial orbits transitioned into the polyhedron-polyhedron model as viewed in a synodic primary-centered frame. Since the orbit of the primary system is not planar or circular, and the orientation of the bodies is time-varying, the primary orientation representation in these figures is only valid at the initial time. Overall, the third body remains on or near the reference trajectory for multiple revolutions, including close encounters with one primary. These simulations demonstrate that trajectories in an idealized model can easily be transitioned into a higher-fidelity dynamical model, assuming the required information about the primary system to construct such a model is in fact available.

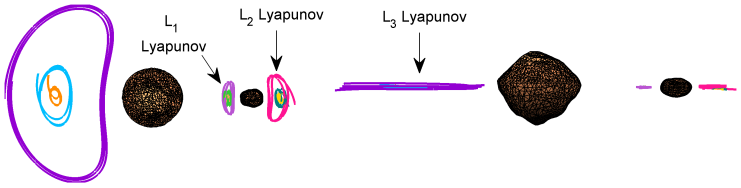

Figure 19. Sample Lyapunov orbits for polyhedron-polyhedron system

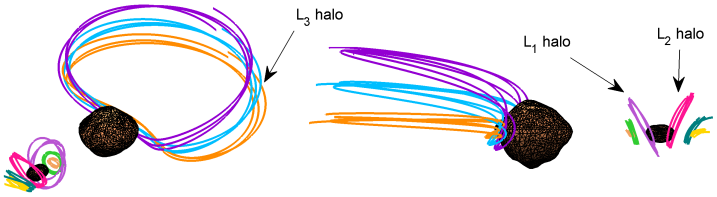

Figure 20. Sample halo orbits for polyhedron-polyhedron system

V. Conclusion

For primary systems that can reasonably be modeled as synchronous, a large survey of third-body periodic trajectories is completed. The catalog that is produced features a wide spectrum of trajectories in terms of dimension, shape, period, and stability properties. Transitioning to dynamical models with incrementally increasing complexity yields results that retain some of the characteristics of the parent simpler model, i.e., the CRTBP, is performed. These trajectories are also subsequently incorporated into an algorithm to construct user-defined tours of the system to explore the regions near the primary bodies. Also, continuation techniques allow such trajectories to be produced for any desired system of bodies that can reasonably be modeled as a pair of ellipsoids. Finally, in an initial assessment of the feasibility and robustness of the trajectories that are constructed leveraging idealized dynamical models, sample trajectories for a known binary system, 1999 KW4, are transitioned into a higher-fidelity dynamical model where each primary body is modeled as a polyhedron and the motion of the primary system reflects the coupling between orbital motion and attitude dynamics. However, such an analysis assumes that detailed knowledge of the primary system

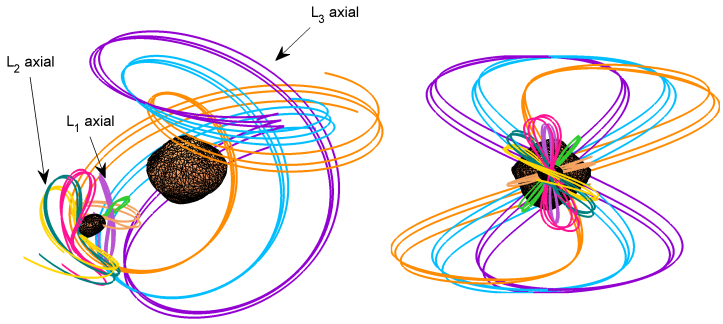

Figure 21. Sample axial orbits for polyhedron-polyhedron system

in terms of the physical and dynamical properties of the primaries is available prior to in situ operations. The authors are currently developing tools to incorporate in the design strategy an autonomous and robust control strategy to maintain a spacecraft in orbit near such reference trajectories based solely on limited knowledge regarding the primary system properties.

VI. Acknowledgment

The authors are extremely grateful to Rune and Barbara Eliasen for their support of this research and funding for the Rune and Barbara Eliasen Visualization Laboratory at Purdue University.

References

[1]Farquhar, R. W., Dunham, D. W., and McAdams, J. V., "NEAR Mission Overview and Trajectory Design, Special Issue on the Near Earth Asteroid Rendezvous Mission," *J. Astronautical Sciences*, Vol. 43, No. 4, 1995, pp. 353–371.

[2]Rayman, M. D., Fraschetti, T. C., Raymond, C. A., and Russell, C. T., "Dawn: A mission in development for exploration of main belt asteroids Vesta and Ceres," *Acta Astronautica*, Vol. 58, June 2006, pp. 605–616.

[3]Marov, M. Y., Avduevsky, V. S., Akim, E. L., Eneev, T. M., Kremnev, R. S., Kulikov, S. D., Pichkhadze, K. M., Popov, G. A., and Rogovsky, G. N., "Phobos-Grunt: Russian sample return mission," *Advances in Space Research*, Vol. 33, Jan. 2004, pp. 2276–2280.

[4]http://osiris-rex.lpl.arizona.edu/. Last accessed 02-23-2013.

[5]Margot, J. L., Nolan, M., Benner, L., Ostro, S., Jurgens, R., Giorgini, J., Slade, M., and Campbell, D., "Binary asteroids in the near-earth object population," *Science*, Vol. 296, 2002, pp. 1445–1448.

[6]Bellerose, J. and Scheeres, D. J., "Periodic orbits in the vicinity of the equilateral points of the restricted full three-body problem," *AAS/AIAA Astrodynamics Specialist Conference*, August 7-11 2005.

[7]Chappaz, L. and Howell, K., "Trajectory Exploration within Binary Systems Comprised of Small Irregular Bodies," *23rd AAS/AIAA Space Flight Mechanics Meeting*, Kauai, Hawaii, February 2013.

[8]Fahnestock, E. G. and Scheeres, D. J., "Simulation and analysis of the dynamics of binary near-Earth Asteroid (66391) 1999 KW4," *Icarus*, Vol. 194, 2008, pp. 410–435.

[9]Fahnestock, E. G. and Scheeres, D. J., "Characterization of Spacecraft and Debris Trajectory Stability within Binary Asteroid Systems," *AIAA/AAS Astrodynamics Specialist Conference and Exhibit*, Honolulu, Hawaii, August 18-21, 2000.

[10]Chappaz, L., "The Dynamical Environment in the Vicinity of Small Irregularly-Shaped Bodies and Application to Asteroids," M.S. Thesis, School of Aeronautics and Astronautics, Purdue University, West Lafayette, Indiana, December 2011.

[11]Bellerose, J. and Scheeres, D. J., "The restricted full three-body problem: Application to binary system 1999 kw4," *Journal of Guidance, Control, and Dynamics*, Vol. 31, No. 1, 2008, pp. 162–171.

[12]Scheeres, D., "Stability of the planar full 2-body problem," *Celestial Mechanics and Dynamical Astronomy*, Vol. 104, No. 1-2, 2009, pp. 103–128.

[13]Lee, T., Leok, M., and McClamroch., N. H., "Lie Group Variational Integrators for the Full Body Problem in Orbital Mechanics," *Celestial Mechanics and Dynamical Astronomy*, Vol. 98, No. 2, 2007, pp. 121–144.

[14]Fahnestock, E. and Scheeres, D., "Simulation of the full two rigid body problem using polyhedral mutual potential and potential derivatives approach," *Celestial Mechanics and Dynamical Astronomy*, Vol. 96, No. 3-4, 2006, pp. 317–339.

[15]Hirabayashi, M. and Scheeres, D., "Recursive computation of mutual potential between two polyhedra," *Celestial Mechanics and Dynamical Astronomy*, Vol. 117, No. 3, 2013, pp. 245–262.

[16]Werner, R. A., "The Gravitational Potential of a Homogeneous Polyhedron or don't Cut Corners," *Celestial Mechanics and Dynamical Astronomy*, Vol. 59, No. 3, 1993, pp. 253–258.

[17]Werner, R. A. and Scheeres, D. J., "Exterior Gravitation of a Polyhedron Derived and Compared with Harmonic and

Mascon Gravitation Representations of Asteroid 4769 Castalia," *Celestial Mechanics and Dynamical Astronomy*, Vol. 65, 1996, pp. 313–344.

[18]Vaquero, M., *Spacecraft Transfer Trajectory Design Exploiting Resonant Orbits in Multi-Body Environments*, Ph.D. thesis, School of Aeronautics and Astronautics, Purdue University, West Lafayette, Indiana, August 2013.

[19]Hadjidemetriou, J. D., "Symmetric and Asymmetric Librations in Extrasolar Planetary Systems: A Global View," *Periodic, Quasi-Periodic and Chaotic Motions in Celestial Mechanics: Theory and Applications*, edited by A. Celletti and S. Ferraz-Mello, Springer, 2006, pp. 225–244.

[20]Jordan, D. W. and Smith, P., *Nonlinear Ordinary Differential Equations: An Introduction to Dynamical Systems*, Oxford University Press Inc., New York, 3rd ed., 1999.

[21]Ostro, S. J., Margot, J.-L., Benner, L. A. M., Giorgini, J. D., Scheeres, D. J., Fahnestock, E. G., Broschart, S. B., Bellerose, J., Nolan, M. C., Magri, C., Pravec, P., Scheirich, P., Rose, R., Jurgens, R. F., De Jong, E. M., and Suzuki, S., "Radar Imaging of Binary Near-Earth Asteroid (66391) 1999 KW4," *Science*, Vol. 314, No. 5803, 2006, pp. 1276–1280.